1

Aromaticity and Antiaromaticity in Nanographenes: An Overview

Albert Artigas and Miquel Solà

Universitat de Girona, Institut de Química Computacional i Catàlisi, Departament de Química, C/Maria Aurèlia Capmany, 69, Girona, 17003 Catalonia, Spain

1.1 Introduction

In 2010, Geim and Novosolev were awarded the Nobel Prize in Physics for the discovery of graphene. Graphene is an allotrope of carbon consisting of a single layer of carbon atoms arranged in a two-dimensional (2D) hexagonal lattice nanostructure, reminiscent of a honeycomb [1]. Despite having remarkable chemical and physical characteristics, its zero band-gap prevents it from being used as a functional material. One way to open this band-gap is the confinement of its electrons in smaller structures called nanographenes, which are tiny fragments of graphene with a minimum size of 1 nm. Nanographenes hold promise for unprecedented physical properties [2], from spin transport [3] to magnetism [4] and from exotic quantum states [5] to stable biexcitonic states [6] (for more information, see the Properties and Applications of Molecular Nanographenes part of this book). By adding defects in the form of 5- to 10-membered rings in the hexagonal lattice, or by the inclusion of sterically strained helical motifs, their structural possibilities can be further extended from the two to the three dimensions in which nanographenes can be chiral [7]. For applications, nanographenes must be structurally perfect and narrow enough. And, of course, they have to be stable. This stability is the result of a combination of several factors such as size, topology, defects, and functionalization. Among these factors, aromaticity plays an important role.

In the realm of aromaticity, misunderstandings and disagreements over its definition and the aromatic nature of specific systems are frequent. Although the concept of aromaticity has been known for nearly two centuries, there is no way to measure it experimentally. The definition of aromaticity has been the subject of numerous studies, reviews, and conferences in the chemical community, although a general consensus has not been reached yet. In a recent perspective [8], some authors even consider that a universal definition of aromaticity is impractical or noncompatible with the general laws constituting chemical theory. Probably, the most accepted definition of aromaticity to date was given in 2005 by Chen et al. [9], who defined this

Molecular Nanographenes: Synthesis, Properties, and Applications, First Edition.
Edited by Nazario Martín and Colin P. Nuckolls.

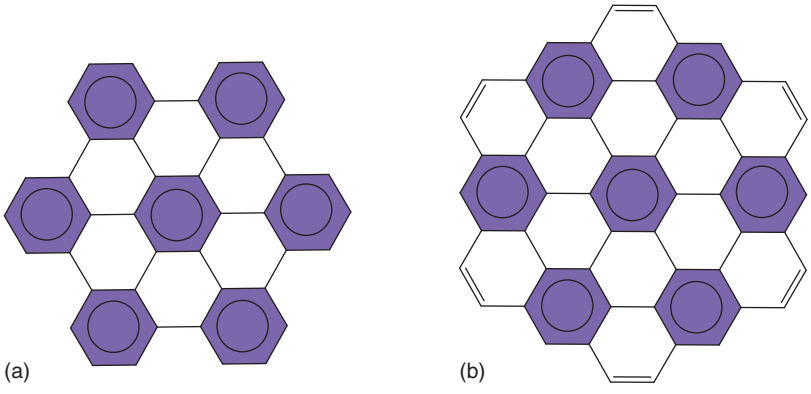

Figure 1.1 The molecular structure of (a) hexabenzocoronene (HBC) and (b) circumcoronene with their Clar π-sextets labeled with a circle in purple.

concept as *"a manifestation of electron delocalization in closed circuits, either in two or in three dimensions. This results in energy lowering, often quite substantial, and a variety of unusual chemical and physical properties. These include a tendency toward bond length equalization, unusual reactivity, and characteristic spectroscopic features"*. It is clear from this definition that electron delocalization and energetic stabilization are the two most fundamental properties of aromatic compounds. The presence of ring currents, symmetry, unusual reactivity, and characteristic spectroscopic features are properties that most aromatic compounds share, but they are not as fundamental as the electron delocalization and stabilization.

Nanographenes are constituted by a relatively large number of rings (most of them six-membered rings, 6-MRs). Hexabenzocoronene (HBC) with 13 6-MRs and circumcoronene with nineteen 6-MRs are still considered polycyclic aromatic hydrocarbons (PAHs), but they are close to the limit (see Figure 1.1). Systems with more than 20 fused 6-MRs can be considered nanographenes, although the frontier between PAHs and nanographenes is fuzzy and smaller systems are often referred as nanographenes in the literature [10].

1.2 Global and Local Aromaticity

Some of the 6-MRs in nanographenes are clearly aromatic and this type of aromaticity is named local aromaticity. Some nanographenes can show important electron delocalization through long circuits and we can refer to this type of aromaticity as global or macrocyclic. This is exemplified in Figure 1.2 for circumcoronene. The local ring currents in the 6-MRs having a Clar π-sextet (vide infra) are undoubtedly identified, together with a global ring current following the perimeter of the molecule that is also clearly depicted.

Clar's π-sextet rule [12] is an empirical guideline that provides a straightforward method for assessing the local aromatic character of individual rings within PAHs. It states that the Kekulé resonance structure with the largest number of disjoint

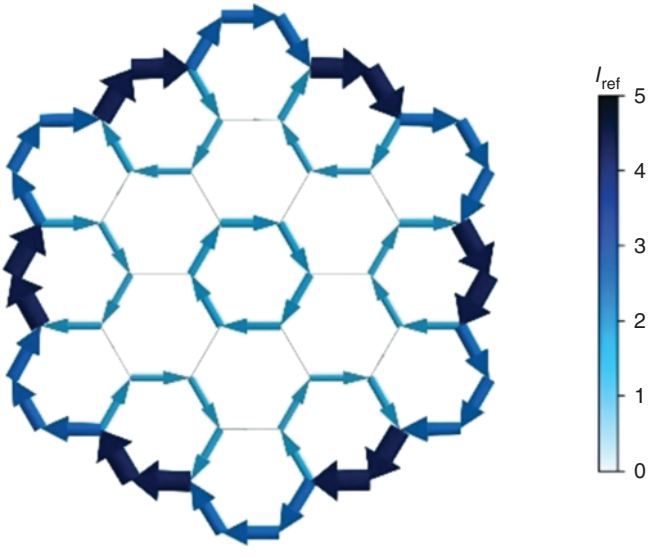

Figure 1.2 The ring currents in circumcoronene computed with the NICS2BC method. Source: Reproduced with permission from Gershoni-Poranne and Tsybizova [11]. John Wiley & Sons.

aromatic π-sextets, that is benzene-like moieties, is the most important resonance structure for the characterization of PAHs (and nanographenes) properties. Aromatic π-sextets were defined by Clar as six π-electrons localized in a single benzene-like ring separated from adjacent rings by formal C—C single bonds. For instance, the application of this rule to phenanthrene indicates that its outer rings are expected to have a higher local aromaticity than the central ring (Figure 1.3). This result was confirmed using different measures of local aromaticity [13]. Clar's π-sextet rule also predicts high stability for HBC of Figure 1.1a because it is made

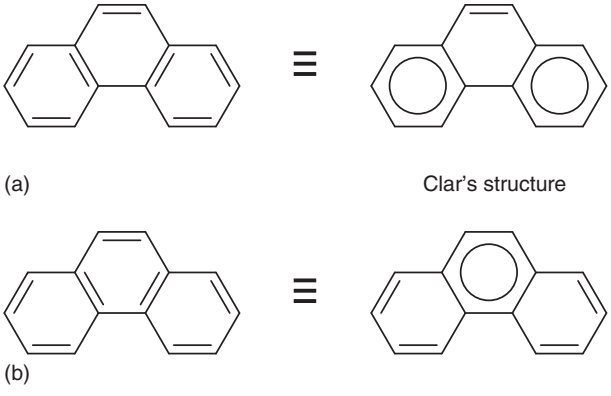

Figure 1.3 Two (a,b) out of the five Kekulé resonance structures of phenanthrene and their corresponding Clar aromatic π-sextets indicated with a circle. The structure with the largest number of aromatic π-sextets is the so-called Clar structure.

only from rings that are either π-sextets or empty rings. These types of systems are called claromatic [14]. In contrast, circumcoronene (Figure 1.1b) has rings with a double bond that are neither π-sextets nor empty rings. These are the most reactive rings and the double bonds are the ones expected to participate, for instance, as dienophiles in Diels–Alder reactions. In 1984, Glidewell and Lloyd proposed to extend the Clar π-sextet rule to nonbenzenoid polycyclic conjugated hydrocarbons (PCHs). Glidewell and Lloyd's rule [15] states that the total population of π-electrons in conjugated polycyclic systems tends to form the smallest $4n + 2$ groups of π-electrons and to avoid the formation of the smallest $4n$ groups.

When discussing the macrocyclic aromaticity, it is essential to refer to an important paper by Anderson and co-workers [16]. In this work, the authors show that by increasing the size of [*N*]annulenes, the aromatic stabilization energy (ASE, see Section 1.3.1) of both aromatic and antiaromatic compounds estimated using the hyperhomodesmotic reaction of Figure 1.4a decreases significantly. Indeed, for $N = 18$, the ASE according to this hyperhomodesmotic reaction is computed to be 8.8 kcal mol^{-1}. The same authors report an experimental ASE for [18]annulene of 2.6 kcal mol^{-1} determined by ^{1}H NMR from the barriers of the exchange of inner and outer protons in [18]annulene [17]. These ASEs are much lower than that of benzene, which is around 30 kcal mol^{-1} depending on the homodesmotic reaction considered [18]. From these results, it is clear that the energetic stabilization due to aromaticity fades away as the ring structure in [*N*]annulenes increases [19]. In an analogous manner, from an energetic point of view, it can be derived that the local aromaticity arising from small circuits in nanographenes is more important

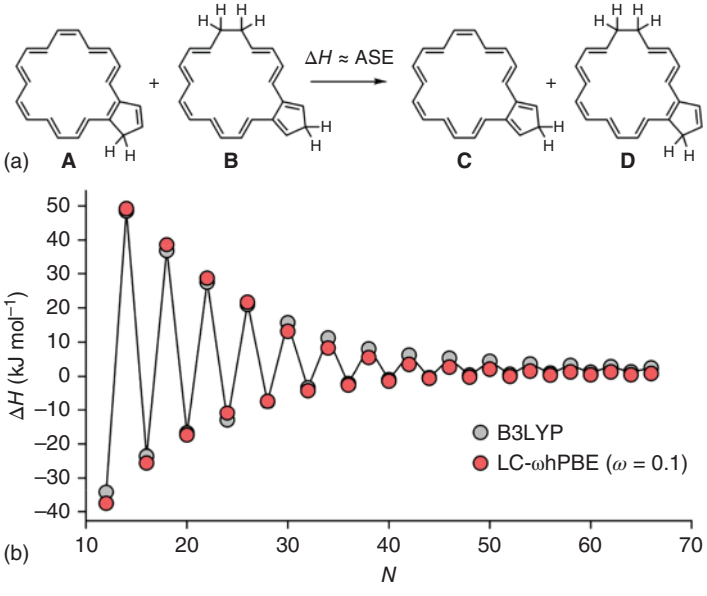

Figure 1.4 (a) A hyperhomodesmotic reaction for estimating the ASE of [*N*]annulenes and (b) values of Δ*H* calculated for this reaction with $N = 12–66$. Source: Reproduced with permission from Jirásek et al. [16]. American Chemical Society.

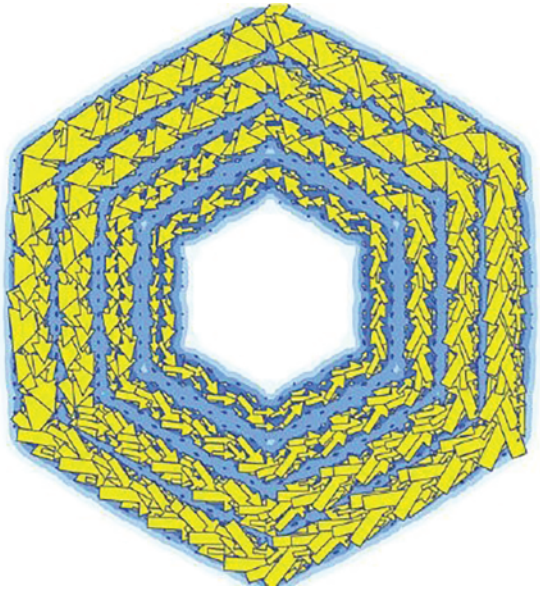

Figure 1.5 Composite maps showing the π-ring currents in D_{6h} [*N*]annulenes (*N* = 30, 42, 54, and 66).
Source: Reproduced with permission from Soncini et al. [20]. Royal Society of Chemistry.

for energetic stability than the presence of long circuits with intense ring currents. As can be seen in Figure 1.5, the intensity of the ring current increases with the size of the [*N*]annulene [20].

In the same line, cyclo[18]carbon, C_{18}, is a very interesting species. C_{18} was characterized by high-resolution atomic force microscopy (AFM) in 2019 [21]. It has two π-conjugated electronic systems described by out-of-plane and in-plane π-molecular orbitals (MOs) that provide different contributions to their stability. Two symmetric geometries can be considered for C_{18}: a nonaromatic D_{9h} polyyne structure with alternating single and triple bonds and a doubly Hückel aromatic cumulenic (D_{18h}) structure having only C=C double bonds (Figure 1.6). From the π-electron counting, C_{18} should be double π_{in} and π_{out} aromatic and, consequently, one should expect the aromatic cumulenic structure as the most stable. However, the AFM study unambiguously established the polyynic structure of C_{18} on the NaCl surface. From a computational point of view, pure and hybrid DFT calculations predict cumulenic structures, whereas Hartree–Fock (HF) and CCSD calculations predict polyynic geometries [22]. In fact, DFT calculated bonding pattern depends on the amount of HF exchange of the hybrid functional (Figure 1.6), with polyynic structure being preferred for functionals with a large percentage of HF exchange [22]. On the other hand, range-separated exchange nonempirical DFT schemes provide polyynic structures regardless of the type of functional used [22]. C_{18} has localized triple bonds and not delocalized double bonds. Consequently, it is not an aromatic molecule neither from an energetic point of view (polyynic more stable than cumulenic structure) nor from the electron delocalization perspective (localized π-electronic structure). However, cyclo[18]carbon would be considered an aromatic macrocycle if one takes into account exclusively the magnetic criteria of aromaticity (see Section 1.3.4 in the chapter). In fact, the magnetic criteria of

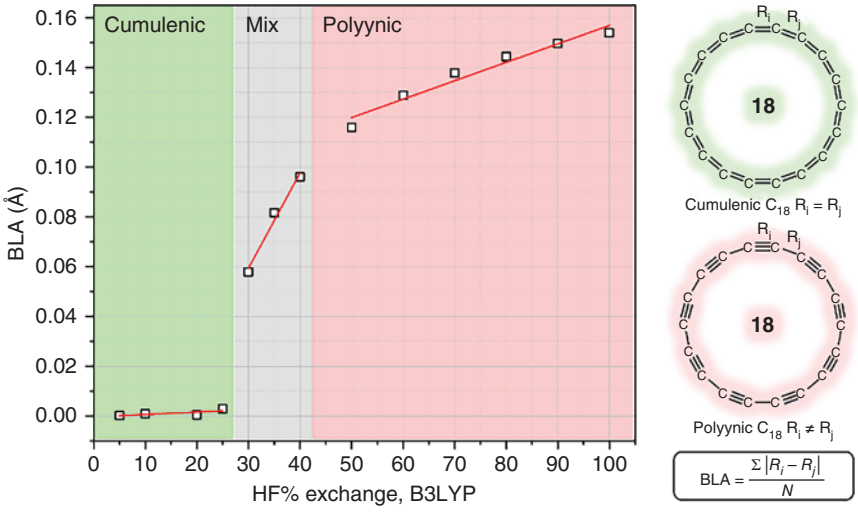

Figure 1.6 Dependence of the bond length alternation (BLA, in Å) in cyclo[18]carbon on the amount of exact exchange in B3LYP functional. Source: Reproduced with permission from Stasyuk et al. [22]. Royal Society of Chemistry.

aromaticity produce incorrect results for cyclo[18]carbon and for most all-carbon rings.

As a whole, we have seen two model macrocyclic systems in which the prediction of aromaticity by magnetic criteria may produce spurious results. This is something that has to be considered when analyzing the global aromaticity of nanographenes. In such cases, the detection of large and intense ring currents may overestimate the global aromaticity of the nanographenes, potentially overshadowing the presence of locally aromatic rings.

As shown by Anderson and co-workers [16], large [*N*]annulenes with $4N + 2$ ($4N$) π-electrons have low positive (negative) ASE. The smallest $4N + 2$ ($4N$) rings are the ones that stabilize (destabilize) the most the PCHs (and nanographenes). This is why the local aromaticity is usually more important than the global aromaticity in nanographenes.

1.3 Methods to Quantify Aromaticity

The quantification of aromaticity is usually based on the fact that aromatic molecules have most of these properties: (i) a continuous cyclic electron delocalization (electronic criteria), (ii) more stability than one would expect (energetic criteria), (iii) bond length equalization (structural criteria), (iv) special response in the presence of magnetic field (magnetic criteria), (v) particular chemical reactivity, and (vi) specific spectroscopic properties. It is generally accepted that one should use a set of indices based on these different properties to discuss the aromaticity of a given species [23]. In the previous section, we have seen that both

energetic and electronic indices are considered fundamental criteria in the analysis of aromaticity. Furthermore, we highlighted that an exclusive reliance on magnetic criteria may yield erroneous conclusions, particularly in the case of large circuits. Consequently, for a comprehensive analysis of aromaticity within a specific system, it is advisable to employ multiple criteria [23], which should include one or more of those classified as fundamental.

1.3.1 Energetic Descriptors of Aromaticity

One of the most important aspects of aromaticity is the energetic stability of the delocalized structure of cyclic-conjugated molecules [18]. A well-known criterion for determining the aromaticity or antiaromaticity of cyclic conjugated compounds is the so-called ASE, which can be determined theoretically or empirically from suitable isodesmic [24] or homodesmotic [25] reactions. Equal numbers of formal single and double bonds are required in products and reactants for isodesmic reactions. In homomodesmotic reactions, which are a subset of isodesmic reactions, the number of bonds between a given atom is the same in each hybridization state. Additionally, the number of hydrogen atoms linked to the atoms in the specific hybridization states must match in reactants and products. The preferred reaction type for estimation of ASE is the homodesmotic because they reduce mistakes caused by strain compensation, anomeric effects, hyperconjugation, etc., [26]. The energy of the substrates and products in these reactions can, in theory, come from thermochemical (calorimetric) observations or from calculations based on quantum chemistry. For instance, the following reaction:

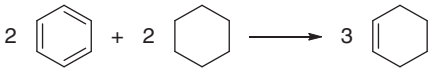

(1.1)

is an example of a homodesmotic reaction that provides an ASE of 37.5 kcal mol^{-1} [18]. Hyperhomodesmotic reactions such as that of Figure 1.4a are homodesmotic reactions in which eight carbon–carbon bond types (H_2C=CH, HC=CH, H_2C=C, HC=C, C=C, HC–CH, HC–C, and C—C) are conserved, constituting a further refinement of homodesmotic reactions [25c].

Schleyer and Pühlhofer [27] were the first to describe the isomerization stabilization energies (ISEs) as a particular approach to obtain ASEs. For a specific (anti)aromatic molecule, the energy difference between a methyl derivative of an annulene and an isomeric species with an acyclic conjugation and an exocyclic methylene group is referred to as ISE. Toluene and a nonaromatic methylenecyclohexadiene can be used to get the ISE for benzene with the following equation:

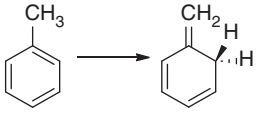

(1.2)

that gives an ISE, and therefore an ASE, of 33.2 kcal mol^{-1} [18].

Due to the strain energy of some of the bonds, determining ASE for nonplanar species is more challenging. Finding a suitable reference structure that completely balances their strain is a major challenge in nonplanar polycyclic conjugated systems, like corannulene. Three formulae that can be used to calculate the ASE of corannulene are shown in Eqs. (1.3)–(1.5) [28]. The B3LYP/6-311G(d,p) level of theory yields ASEs of 37.7 and 42.5 kcal mol^{-1} for the first two reactions. The homodesmotic requirements are met by the two reactions. Varied numbers of *syn* and *anti* butadiene subunits and varied numbers of H· · ·H repulsive interactions can be used to explain the 4.8 kcal mol^{-1} discrepancy between the two reactions. The calculated ASE for reaction (1.5) is more balanced in terms of *syn*/*anti* units and H· · ·H interactions, so the estimated ASE using this reaction of 46.7 kcal mol^{-1} is more precise.

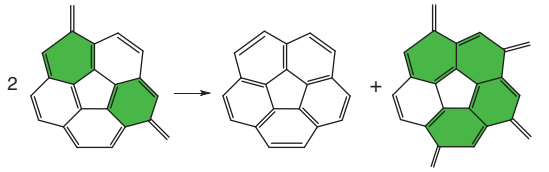

(1.3)

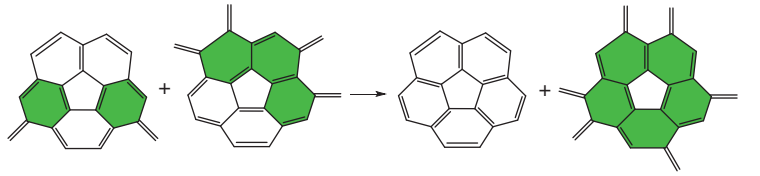

(1.4)

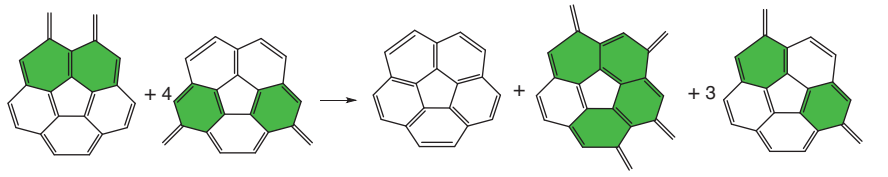

(1.5)

Similar equations have been designed to estimate the ASE of fullerenes (results show that the cyclic π electron delocalization does not stabilize C_{60} [29]), nonplanar linear acenes [30], and highly bent pyrenophane [31]. Still, it is not an easy task to design reactions to estimate the ASE of nanographenes. The advantages and drawbacks of ASE are the following:

Strengths

- The thermodynamic stabilization due to aromaticity is the most important primary effect of aromaticity.
- It can classify aromatic, nonaromatic, and antiaromatic species.

Weaknesses

- The design of proper homodesmotic reactions is not easy, especially in the case of large nanographenes.
- Separation into α and β components is not possible.
- Separation into $\pi/\sigma/\delta\ldots$ contributions is not possible.

- Not always possible to separate local and global aromaticity.
- It cannot be used to find the most favorable circuit for electron delocalization.

1.3.2 Electronic Descriptors of Aromaticity

The cyclic delocalization of mobile electrons in two or three dimensions is one of the fundamental and essential properties of aromatic compounds. There is no experimental characteristic that allows for the direct measurement of this electronic delocalization because it is not observable. For this reason, there is no single, consensual way to measure it theoretically. There are many electronic descriptors of aromaticity [32], and we just list a few of the most popular ones here.

The delocalization index (DI) between atoms A and B, $\delta(A,B)$, provides a measure of the number of electrons shared by atoms A and B [33]. For monodeterminantal closed-shell wavefunctions, is obtained from Eq. (1.6),

$$\delta(A,B) = 4 \sum_{i,j}^{\text{occ.MO}} S_{ij}(A) S_{ij}(B) \tag{1.6}$$

The summation in Eq. (1.6) runs over all occupied molecular orbitals. $S_{ij}(A)$ is the overlap between molecular orbitals i and j within the basin of atom A. Delocalization indexes in Eq. (1.6) reduce to Wiberg–Mayer bond orders [34] if the integrations over atomic basins are replaced by a Mulliken-like partitioning of the corresponding integrals. For planar species, $S_{ij}(A_k) = 0$ for $i \in \sigma$ and $j \in \pi$ orbital symmetries, thus the DI can be exactly split into σ- and π-contributions.

The aromatic fluctuation index (FLU) [35] takes into account the uniformity of the electron delocalization along the molecular ring and its difference with respect to some aromatic reference, Eq. (1.7):

$$\text{FLU}(A) = \frac{1}{N} \sum_{i=1}^{N} \left[\left(\frac{V(A_i)}{V(A_{i-1})} \right)^{\alpha} \left(\frac{\delta(A_i, A_{i-1}) - \delta_{\text{ref}}(A_i, A_{i-1})}{\delta_{\text{ref}}(A_i, A_{i-1})} \right) \right]^2 \tag{1.7}$$

where the ring considered is formed by atoms in the string $\{\boldsymbol{A}\} = \{A_1, A_2, \ldots A_N\}$, $A_0 \equiv A_N$ and the atomic delocalization is defined by Eq. (1.8),

$$V(A) = \sum_{A \neq B} \delta(A,B) \tag{1.8}$$

In Eq. (1.8), α is a function that ensures that the ratio of atomic delocalizations is always greater or equal to 1,

$$\alpha = \begin{cases} 1 & V(A_i) > V(A_{i-1}) \\ -1 & V(A_i) \leq V(A_{i-1}) \end{cases} \tag{1.9}$$

The reference values of C—C and C—N bonds are taken from benzene and pyridine in their ground state. FLU is very close to 0 in aromatic rings and rises as the aromaticity of the rings decreases. The strengths and weaknesses of FLU are the following:

Strengths

- Electron delocalization is a primary property of aromaticity.

- Separation into α and β components is possible.
- There is a FLU_{π} version of this index that can be applied to planar π-conjugated species that does not require reference values.
- In macrocycles or nanographenes, FLU can be used to find the most favorable circuit for electron delocalization.

Weaknesses

- It cannot be applied to structures far from equilibrium (e.g. transition states).
- It cannot be applied to structures having bonds in the ring with no reference values.
- As reference values are derived for the ground states, caution must be taken when applying FLU to excited states.
- It cannot easily differentiate between nonaromatic and antiaromatic compounds.

The delocalization index can be generalized to study multicenter bonding by defining a multicenter delocalization index (I_{ring}) among the N centers A_1 to A_N. These A_1 to A_N atoms can be atoms of a ring ($A_0 \equiv A_N$) but also could be N selected atoms not necessarily involved in a ring. According to Giambiagi and coworkers [36], the form of this index for monodeterminantal closed-shell wavefunctions is given by Eq. (1.10),

$$I_{ring}(A) = 2^N \sum_{i_1,i_2,i_3\ldots,i_N}^{OCC} S_{i_1 i_2}(A_1) S_{i_2 i_3}(A_2) \ldots S_{i_N i_1}(A_N) \tag{1.10}$$

Bultinck and coworkers defined the multicenter index, MCI [37], as an extension of the I_{ring} index with the formula:

$$MCI(A) = \frac{1}{2N} \sum_{P(A)} I_{ring}(A) = \frac{1}{2N} \sum_{P(A)} \sum_{i_1,i_2,i_3\ldots,i_N}^{OCC} S_{i_1 i_2}(A_1) S_{i_2 i_3}(A_2) \ldots S_{i_N i_1}(A_N) \tag{1.11}$$

where *P(A)* represents all possible permutations among centers A_1 to A_N and the internal summation runs over all occupied molecular orbitals. Both I_{ring} and MCI give a measure of the electron sharing through the whole studied ring. The more aromatic the ring is, the more positive the I_{ring} and MCI are. The size of the ring affects the values of I_{ring} and MCI; their values decrease with increasing ring size. There is a normalized version of the I_{ring} and MCI indexes, the so-called I_{NG} and I_{NB} [38] indexes, to reduce or avoid this problem. The I_{ring} and MCI have the following strengths and weaknesses:

Strengths

- Electron delocalization is a primary property of aromaticity.
- Separation into α and β components is possible.
- They have no reference values and, therefore, they can be applied to species containing any type of atom.
- I_{ring} and MCI are considered the most precise ways to quantify aromaticity by some authors [39].

Weaknesses

- It cannot easily differentiate between nonaromatic and antiaromatic compounds.
- When using QTAIM partitioning [40], it can only be used for small to medium-sized rings (fewer than 12 atoms) due to numerical inaccuracies.
- They have a high computational cost for large rings, especially MCI.
- In general, due to its computational cost, I_{ring} and MCI cannot be used to find the most favorable circuit for electron delocalization.
- They are size dependent. The larger the ring, the smaller the value. However, this can be solved using the normalized version of these indices, I_{NG} and I_{NB}, or in a simpler way using $MCI^{1/N}$ and ${I_{ring}}^{1/N}$ with N being the number of atoms of the ring.

The electron localization function (ELF) has so far been demonstrated to be a useful tool for locating electron pairs. As a result, the ELF has been extensively employed to explain the process of chemical reactions and comprehend the nature of chemical bonding [41]. The definition of the ELF by Becke and Edgecombe [42] is based on the spherically averaged same-spin conditional pair density. The ELF can be expressed as:

$$\mathrm{ELF} \equiv \quad \eta = \frac{1}{1 + D(\vec{r})^2} = \frac{1}{1 + \left(\frac{D_\sigma}{D_\sigma^0}\right)^2} \tag{1.12}$$

where D_σ reveals the excess kinetic energy density of the σ electrons ($\sigma = \alpha$ or β) caused by Pauli repulsion and the D_σ^0 can be interpreted as Thomas–Fermi kinetic energy density.

The ELF is defined to range the electron localization measure in the interval [0,1] with a Lorentzian form. ELF = 1 corresponds to a completely localized situation, 0 to corresponds to a delocalized one, and ELF = 0.5 is the value one should obtain for the homogenous electron gas. A volume that is enclosed by an isosurface whose value is determined by the ELF is known as a localization domain. If a localization domain has more than one attractor, it is said to be reducible. When the ELF value defining a reducible localization domain is raised, this latter splits into two new domains that share a (3,−1) critical point. A bifurcation point is the ELF value where a domain splits in two and the value of ELF at which two basins merge is called a bifurcation value (BV). Figure 1.7 depicts the localization domains and bifurcation diagram of the benzene molecule. On the left side of Figure 1.7, the localization domains of benzene bounded by the ELF($\mathbf{r}$) = 0.65 isosurface characterized by the aromatic domain in green are shown, whereas on the right side, the bifurcation diagram is presented. In this latter, the successive bifurcations occur for ELF($\mathbf{r}$) = 0.1 (core-valence), 0.61 (V[C,H] from aromatic domain) and 0.65 (aromatic domain).

The ring-closure bifurcation value (RCBV) is the ELF value at which all basins in the ring merge to form one continuous cyclic basin. The π-component of the electron localization function (ELF_π) can be computed using only the occupied π molecular orbitals and the π density [43]. These two properties are required to consider a system aromatic: (i) the maximal difference between the bifurcation values,

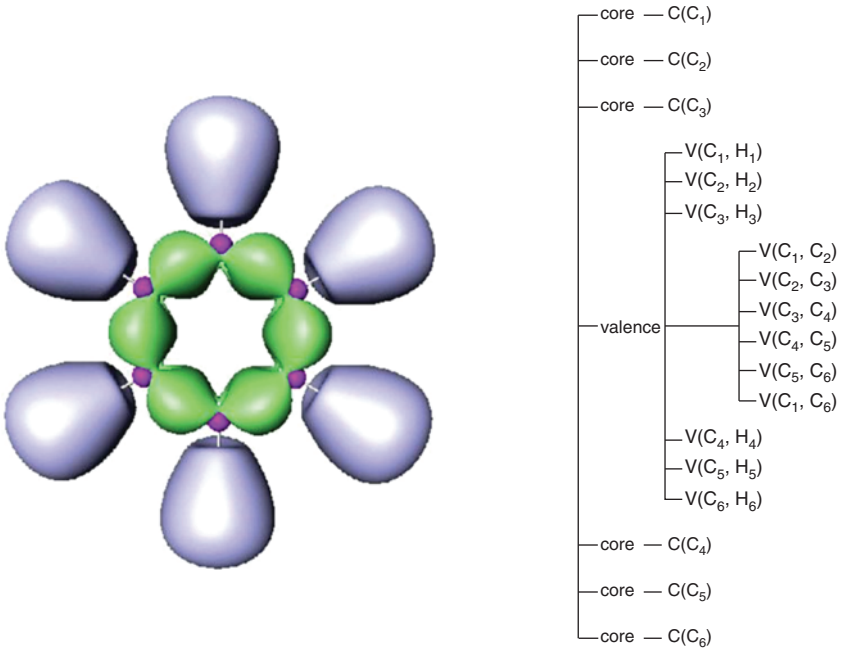

Figure 1.7 Localization domains and bifurcation diagram of the benzene molecule. Core C(C) domains in magenta, valence V(C,C) domains in green and valence V(C,H) domains in purple. Source: Reproduced with permission from Poater et al. [41]. American Chemical Society.

$\Delta BV(ELF_\pi)$ should be small and (ii) the $RCBV(ELF_\pi)$ should be above a certain threshold (0.64–0.70) [43]. The strong and weak points of ELF are:

Strengths

- Electron delocalization is a primary property of aromaticity.
- Separation into α and β components is possible.
- It has no reference values and, therefore, they can be applied to species containing any type of atom.
- It can be visualized.

Weaknesses

- It cannot easily differentiate between nonaromatic and antiaromatic compounds.
- ELF_π requires the molecule to be planar.
- It cannot be easily applied to differentiate between local and global aromaticity.
- There are no examples of using ELF_π to determine the most favorable circuit for electron delocalization.

The localized orbital locator (LOL) [44] is a function closely related to ELF and its variant, LOL-π, has been also successfully used to investigate delocalization channel of π electrons [45].

The electron density of delocalized bonds (EDDB) method decomposes the one-electron density in several "layers" corresponding to different levels of electron

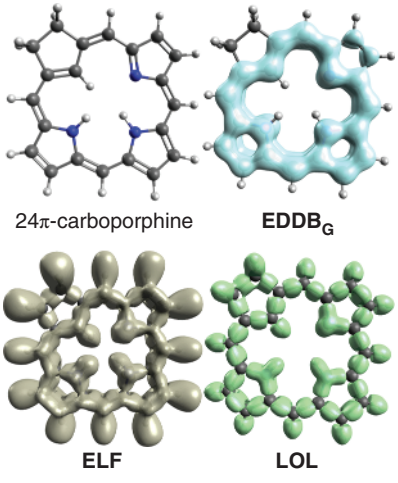

Figure 1.8 Plot of the global aromaticity of 24π-electron carboporphine visualized by EDDB$_G$, ELF, and LOL with the CAM-B3LYP/6-311G(d,p) method. Source: Reproduced from Szczepanik and Solà [48]/with permission of ELSEVIER.

delocalization [46], namely, the electron density of localized atoms (EDLA) representing inner shells, lone pairs, etc.; the electron density of localized bonds (EDLB) representing typical (two-center two-electron) Lewis-like bonds; and EDDB, which represents electron density that cannot be assigned to atoms or bonds due to its (multicenter) delocalized nature. The EDDB population of electrons delocalized in a 2D or three-dimensional (3D) closed circuit can be used as an indicator of aromaticity [47]. Regardless of their size, topology, or electronic state, electrons delocalized across the system of all (global) or particular (local) conjugated bonds in a variety of (aromatic) species can be quantified and visualized using the EDDB function. Figure 1.8 depicts the global EDDB for 24π-electron carboporphine. It is clear from the picture the local aromaticity of the pyrrole rings that provides most of the ASE. Strengths and weakness of EDDB are:

Strengths

- Electron delocalization is a primary property of aromaticity.
- Separation into α and β components as well as $\pi/\sigma/\delta\ldots$ contributions is possible.
- It has no reference values and, therefore, it can be applied to species containing any type of atom.
- It can be visualized.
- In macrocycles or nanographenes, EDDB can be used to find the most favorable circuit for electron delocalization.
- It is fast to compute.
- It can be easily applied to differentiate between local and global aromaticity.

Weaknesses

- It cannot easily differentiate between nonaromatic and antiaromatic compounds.

1.3.3 Geometric Descriptors of Aromaticity

The geometric definition of aromaticity is based on the reduced difference in bond lengths between unsaturated acyclic analogs and aromatic compounds. The most

used descriptor derived from chemical structures is the harmonic oscillator model of aromaticity (HOMA) index. It can be obtained from the following expression [49]:

$$\begin{aligned} \mathrm{HOMA} &= 1 - \frac{\alpha}{n}\sum_{i=1}^{n}(R_{\mathrm{opt}} - R_i)^2 = 1 - \left[\alpha(R_{\mathrm{opt}} - R_{\mathrm{av}})^2 + \frac{\alpha}{n}\sum_{i=1}^{n}(R_{\mathrm{av}} - R_i)^2\right] \\ &= 1 - \mathrm{EN} - \mathrm{GEO} \end{aligned} \tag{1.13}$$

where n is the number of bonds considered and α is an empirical constant selected to give HOMA = 0 for a nonaromatic model system. When HOMA = 1, the system with all bonds equal to an optimal R_{opt} value is assumed to be fully aromatic. For C—C, C—N, C—O, N—N [49c], C—B [50], and B—B [51] bonds, α = 257.7, 93.5, 157.4, 130.3, 104.5, and 244.1, whereas R_{opt} = 1.388, 1.334, 1.265, 1.309, 1.424, and 1.567 Å, respectively. R_i stands for a running bond length and R_{av} is the mean bond length of the ring. HOMA value can be divided into energetic (EN) and geometric (GEO) contributions [49c, 52], according to the relationship HOMA = 1 – EN – GEO (Eq. (1.13)). While the EN term accounts for the lengthening/shortening of the ring's mean bond lengths, the GEO contribution reflects changes in bond length alternation (BLA). For HOMA, we can list the following strengths and weaknesses:

Strengths

- In macrocycles or nanographenes, it can be used to find the most favorable circuit for electron delocalization.
- It can classify aromatic, nonaromatic, and antiaromatic species.
- Applicable to structures derived from experiments and theory.
- It is possible to analyze local and global aromaticity.

Weaknesses

- Separation into α and β components is not possible.
- Separation into $\pi/\sigma/\delta\ldots$ contributions is not possible.
- It cannot be applied to structures far from equilibrium (e.g. transition states) or excited states.
- It cannot be applied to structures having bonds in the ring with no reference values.

1.3.4 Magnetic Descriptors of Aromaticity

When a metallic loop is subjected to an external magnetic field ($\vec{B}_{\mathrm{o}}$), an electric current is induced following the Faraday's law of induction. This electric current generates an induced magnetic field ($\vec{B}_{\mathrm{ind}}$) that opposes the external magnetic field and is proportional to the external magnetic field ($\vec{B}_{\mathrm{o}}$) as shown in Eq. (1.14),

$$\vec{B}_{\mathrm{ind}} = -\vec{\vec{\sigma}}\vec{B}_{\mathrm{o}} \tag{1.14}$$

where $\vec{\vec{\sigma}}$ is the magnetic shielding tensor defined by Eq. (1.15):

$$\sigma_{\alpha\beta} = \frac{\partial^2 E}{\partial\mu_\alpha \partial B_\beta} \tag{1.15}$$

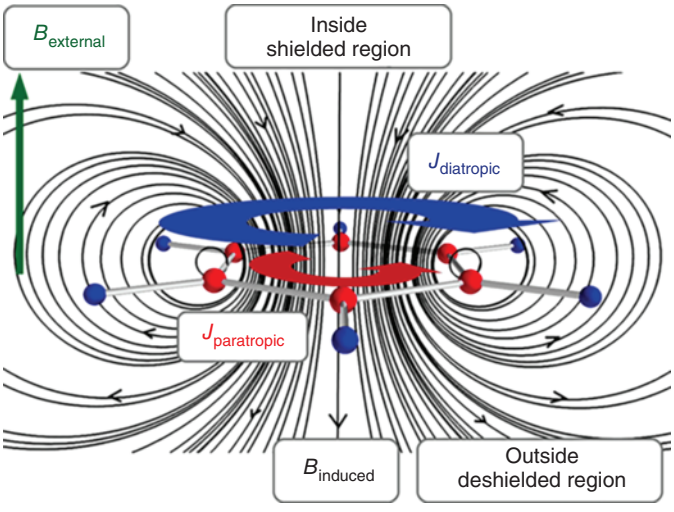

Figure 1.9 The diatropic (clockwise, blue) and paratropic (anticlockwise, red) directions of the induced current flow relative to the external magnetic field (green) using benzene as an example. Source: Reproduced with permission from Sundholm et al. [53]/John Wiley & Sons.

with E being the electronic energy of the molecule, $\boldsymbol{B}$ the external magnetic field, and $\boldsymbol{\mu}$ the magnetic moment (in a loop $\mu = I.A$, intensity per area). This shielding tensor of nine components is symmetric ($\sigma_{\alpha\beta} = \sigma_{\beta\alpha}$, with α and $\beta = x, y, z$) and different at each point in space. Aromatic molecules contain delocalized electrons in a closed cyclic circuit, and, therefore, in the presence of an external magnetic field, these molecules show a ring current and the corresponding induced magnetic field (see Figure 1.9). The magnetic shielding tensor, $\vec{\vec{\sigma}}$, computed at the center of the aromatic ring provides an estimation of the intensity of the ring currents induced by the external magnetic field.

By applying the first-order response to the applied magnetic field, the current density J($\mathbf{r}$) of the ring current induced by the external field is given by [53]:

$$J(\vec{r}) = \frac{i}{2}(\Psi_R \nabla\Psi_I - \Psi_I \nabla\Psi_R + 2i\Psi_R A(\vec{r})\Psi_R) \tag{1.16}$$

where $\mathbf{A}(\mathbf{r}) = \frac{1}{2}\mathbf{B_0}\mathrm{x}(\mathbf{r} - \mathbf{R_0})$ is a vector potential for the external magnetic field. In the presence of an external magnetic field, the total wavefunction $\Psi(\mathbf{r})$ is composed of a real, Ψ_R, and an imaginary, Ψ_I, component. The first two terms in Eq. (1.16) are the paramagnetic contribution to the ring current and the last term is the diamagnetic one. The calculated ring currents are origin dependent. Several attempts have been performed to circumvent the gauge origin problem. Among them, the gauge-including magnetically induced currents (GIMIC) method has been one of the most widely used [54]. As can be seen in Figure 1.9, in benzene, the ring currents show a strong diatropic ring current outside the ring and a less intense paratropic one inside the ring. To obtain more detailed information about current pathways and strengths in nanographenes, one can determine by numerical integration the

current strength for each bond. Ring currents are not observable, but their effects are (in NMR spectra, for instance).

Strengths and weaknesses of ring currents are:

Strengths

- Separation into α and β and $\pi/\sigma/\delta\ldots$ contributions is possible.
- They have no reference values and, therefore, they can be applied to species containing any type of atom.
- They can be visualized.
- Results of NMR chemical shifts, which can be calculated from ring currents, can be obtained experimentally and compared.
- In macrocycles or nanographenes, ring currents can be used to find the most favorable circuit for electron delocalization.
- They can easily differentiate between aromatic, non-aromatic, and antiaromatic compounds.

Weaknesses

- The size of the ring can influence the ring's current strengths.
- Ring currents can indicate aromaticity in large macrocycles that are in fact nonaromatic.
- For systems with small HOMO–LUMO gaps, the (anti)aromaticity can be overestimated due to the high intensity of the ring currents.
- Ring currents are likely to be overestimated in excited states because of small energy differences between frontier orbitals.
- Application to radical species or to $\sigma\pi^*$ or $\pi\sigma^*$ excited states may produce spurious results because of the small SOMO–LUMO gaps.
- In some cases, contributions from electrons not related to aromaticity (e.g. σ-electrons in classical aromatic compounds) can be important.

Another widely used method to analyze aromaticity in nanographenes is the so-called anisotropy of the magnetically induced current density tensor (anisotropy of the induced current density, ACID). ACID was proposed by Herges and Geuenich [55] as a scalar function that can be used to determine the degree of electron delocalization of molecules [56]. The ACID quantity is defined as:

$$\Delta J^2(\vec{r}) = \frac{1}{3}\left[\left(J_x^x(\vec{r}) - J_y^y(\vec{r})\right)^2 + \left(J_y^y(\vec{r}) - J_z^z(\vec{r})\right)^2 + \left(J_z^z(\vec{r}) - J_x^x(\vec{r})\right)^2\right] + \frac{1}{2}\left[\left(J_x^y(\vec{r}) - J_y^x(\vec{r})\right)^2 + \left(J_x^z(\vec{r}) - J_z^x(\vec{r})\right)^2 + \left(J_y^z(\vec{r}) - J_z^y(\vec{r})\right)^2\right] \quad (1.17)$$

The ACID function (Figure 1.10) is usually depicted in yellow and on top of the surface, one plots the ring currents. ACID share the same strengths and weaknesses as the ring currents with the following additional weaknesses:

Additional Weaknesses

- In many cases, the direction of the ring currents is not clearly seen and researchers plot their own arrows to indicate the diatropic or paratropic circulations.
- For very symmetric 3D-aromatic structures, such as in *closo* boranes, the different $J_\beta^\alpha(\vec{r})$ components of the induced current density tensor are very similar and

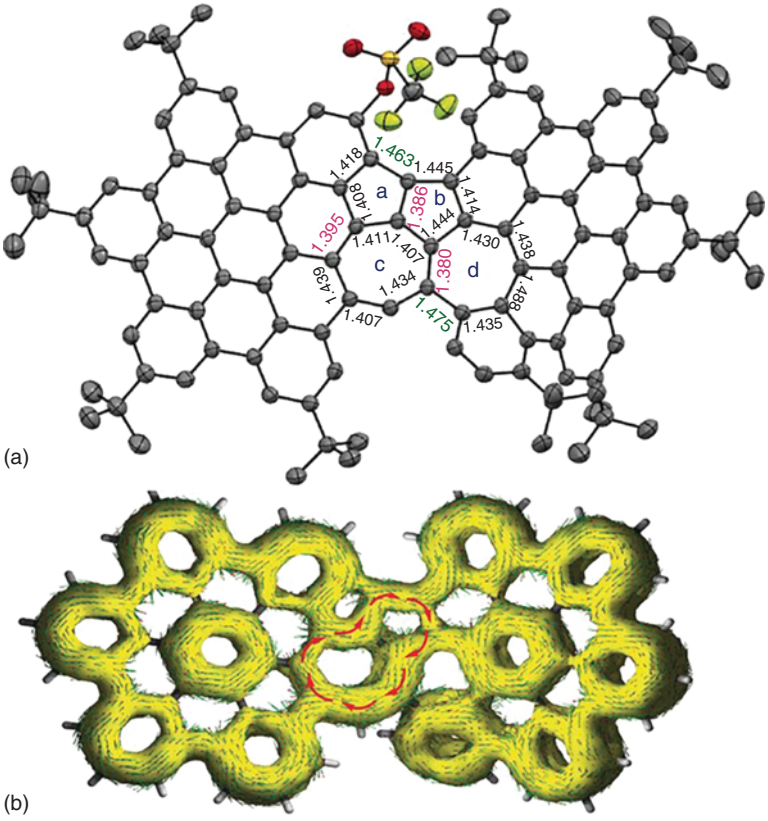

Figure 1.10 (a) X-ray crystallographic structure of a nanographene with selected bond lengths (in Å). (b) Calculated ACID plot of the backbone, with the added red arrows showing diatropic ring current flow along one azulene unit; the external magnetic field is applied orthogonally to the plane of the ring. Source: Reproduced from Han et al. [57]/with permission of John Wiley & Sons.

the anisotropy of the magnetically induced current density tensor is close to zero. Therefore, ACID is zero despite the system being aromatic.

Probably the most broadly used indicator of aromaticity is the nucleus independent chemical shift (NICS) [9, 58]. It is defined as the negative value of the absolute isotropic shielding computed at the center of a ring or at some other point of the system. It is obtained by averaging the diagonal elements of the magnetic shielding tensor in Eq. (1.15) over all directions, as shown in Eq. (1.18):

$$\mathrm{NICS} = -\frac{1}{3}(\sigma_{xx} + \sigma_{yy} + \sigma_{zz}) = -\sigma_{av} \tag{1.18}$$

NICS can be computed at any point in space. The center of aromatic rings has negative NICS values (NICS(0)). The more aromatic the ring is, the more negative the NICS value is. To remove the effect of σ-electrons that are not related to aromaticity, one can use NICS(1), that is the NICS value at 1 Å above or below the center of the ring plane. NICS(1) is considered to better reflect the π-electron effects [59]. One can

also use the out-of-plane tensor component of NICS(1), that is $NICS(1)_{zz}$. Another choice is to employ the π contribution to the out-of-plane magnetic shielding tensor component computed at the center of the ring or at 1 Å above or below the ring plane ($NICS(0)_{\pi zz}$ and $NICS(1)_{\pi zz}$, respectively). $NICS(1)_{zz}$ and $NICS(0)_{\pi zz}$ have been considered the best measures of aromaticity in organic compounds [39a, 60] among numerous NICS-related definitions. Although widely used, NICS is not exempt from criticism [61].

The NICS value at a particular position in nanographenes with several fused rings that may contain multiple induced current circuits may be the result of various induced magnetic fields [61h]. Couplings of different induced magnetic fields could result in incorrect (anti)aromaticity assignments for the systems under study. For the determination of local and global ring currents in polycyclic conjugated hydrocarbons and nanographenes, Gershoni-Poranne and Stanger [62] developed the NICS-based technique known as the NICS-XY-scan. The procedure entails positioning the NICS probes (commonly referred as *Bq*) along the *X* axis and, as necessary, along the *Y* axis at a fixed *Z* height (the authors recommend 1.7 Å) above the system being investigated (Figure 1.11a). Identification of both global and local induced currents is possible by tracking changes in the NICS values along these axes.

A 3D grid of NICS probes was used by Klod and Kleinpeter [66] to draw an iso-chemical-shielding surface (ICSS, see Figure 1.11b) for the first time in 2001. These plots depict the effects of ring current-induced shielding and deshielding in various molecular locations (Figure 1.11b). Aromatic compounds exhibit the characteristic shielding cone, such as benzene or C_{60}^{6-} [63]. If the external magnetic field ($\vec{B}_o$) perpendicular to the ring is assumed to be 1 T, profiles of $\vec{B}_{ind}$ or $\vec{B}_{ind}^{z}$ are equivalent to those of the NICS or $NICS_{zz}$ index, as can be seen from the application of Eq. (1.14) [67]. In this sense, 3D plots of induced magnetic fields are equivalent to ICSSs.

Lampkin, Karadakov, and Vanveller introduced a method for depicting isotropic magnetic shielding (IMS, the negative of NICS), across a 2D array of *Bq* positioned at varying distances from the molecular plane of (anti)aromatic molecules, including PAHs [65]. This approach yields visually captivating contour maps that facilitate a clear and appealing visualization of electron delocalization, possibly evoking the concept of Clar π sextets in PAHs (Figure 1.11c). 2D IMS maps represent essentially cross-sections of the ICSS and for this reason, they are commonly referred to as "2D ICSS" in the literature. To end, Coquerel, Carissan et al. [68] have proposed a variation of these contour maps that represent the IMS three-dimensionally over *pseudo van der Waals* surfaces made of *Bq* constructed around a given molecule. This method serves as a potent alternative to ICSS and 2D IMS maps, especially when dealing with intricately contoured 3D nanographene systems, and retains the intuitive and visual aspects of its 2D counterparts (refer to Figure 1.11d).

The strengths and weaknesses of NICS and related measures are the following:

Strengths

- Separation into α and β and $\pi/\sigma/\delta\ldots$ contributions is possible.

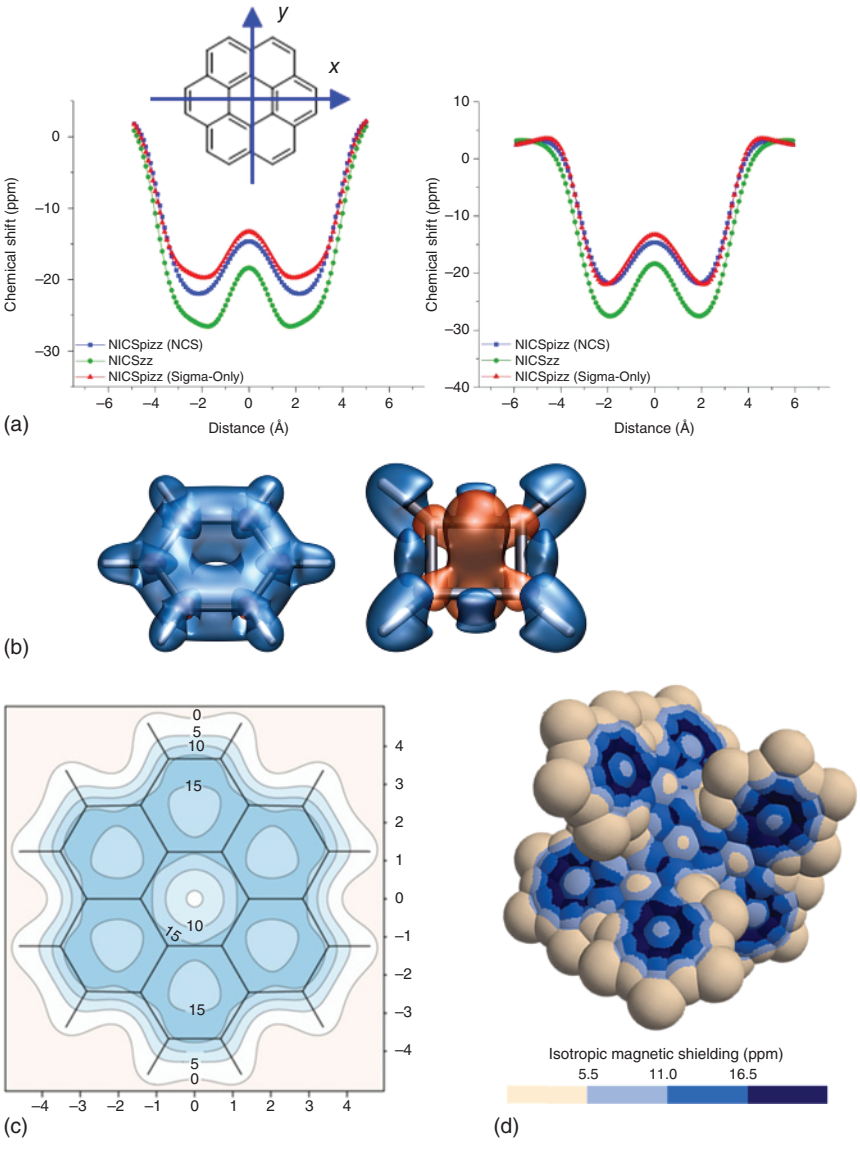

Figure 1.11 (a) The NICS-XY-scan method applied to coronene along the *X* axis (left) and the *Y* axis (right). Source: Adapted from Muñoz-Castro [63]. (b) Isotropic shielding and deshielding surfaces of benzene (left) and butadiene (right). Source: Reproduced with permission from Karadakov et al. [64]. American Chemical Society. (c) IMS contour map of coronene (***B*** at 1 Å distance from the molecular plane). Source: Reproduced with permission of Lampkin et al. [65], 2020 John Wiley & Sons. (d) 3D IMS map of hexabenzotriphenylene.

- It has no reference values and, therefore, it can be applied to species containing any type of atom.
- Plots of NICS can be visualized.
- It can easily differentiate between aromatic, nonaromatic, and antiaromatic compounds.
- It is one of the easiest to calculate indicators of aromaticity. It is available in most quantum chemistry programs.
- The modern versions of this index such as $NICS_{zz}$, $NICS_{\pi}$, NICS scans, or NICS-XY-scan provide reliable results in most cases.

Weaknesses

- The size of the ring influences the NICS values.
- NICS values can indicate aromaticity in large macrocycles that are in fact nonaromatic.
- For systems with small HOMO–LUMO gaps, the (anti)aromaticity can be overestimated by NICS due to the high intensity of the ring currents.
- NICS is likely to be overestimated in excited states because of small energy differences between frontier orbitals.
- Application to radical species may produce spurious results because of the small SOMO–LUMO gaps.
- Application to $\sigma\pi^*$ or $\pi\sigma^*$ excited states with an unpaired number of π-electrons may produce overestimated (anti)aromaticities because of the small SOMO–LUMO gaps.
- In some cases, contributions from electrons not related to aromaticity (e.g. σ-electrons in classical aromatic compounds) can be important.
- In PAHs and nanographenes, the influence of the induced magnetic fields of adjacent rings can be substantial.
- NICS can indicate the aromaticity of systems that are not aromatic such as $(HF)_3$ [61e], carborane-fused rings or large macrocycles.

1.4 The Analysis of Aromaticity in Nanographene Systems

So far, in this chapter we have seen that aromaticity is a contentious concept, encompassing numerous criteria that, consequently, have given rise to an assorted variety of computational approaches for assessing the (anti)aromatic character of molecules. As a result, using different methods or criteria may lead to conflicting outcomes. An obvious recommendation would be to use at least two different methods or criteria based on different properties when evaluating the global and/or local aromaticity of a particular system, and, if possible, at least one of them should be based on energetic or electron delocalization measures. The advantages and disadvantages outlined in the preceding section may serve as valuable guidelines for selecting the most suitable ones. In this section, we will discuss some illustrative examples of how some of the methods introduced in Section 1.3 have been employed in recent

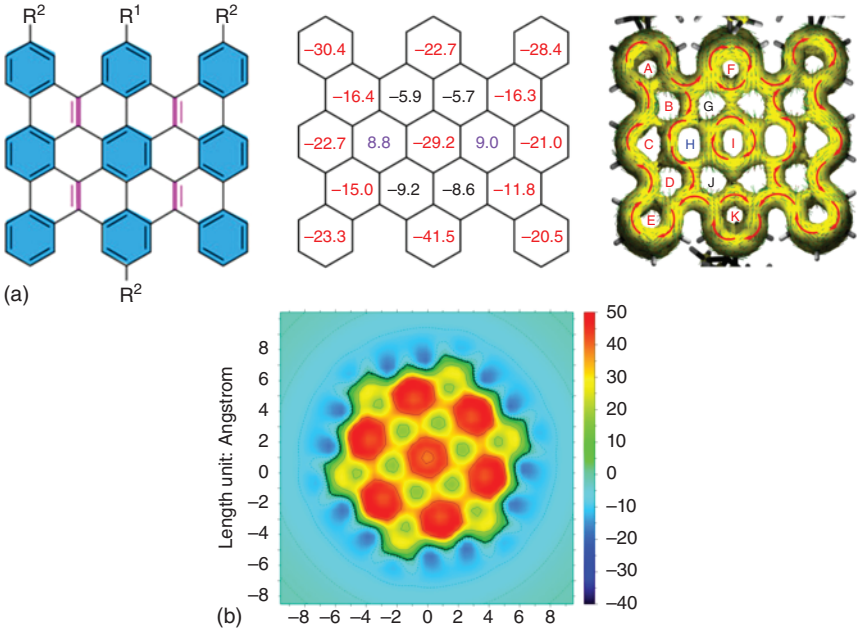

Figure 1.12 (a) A cove-edged (Clar π-sextets highlighted in blue) and the analysis of its aromaticity by the single-point NICS and ACID methods. Source: Reproduced from Gu et al. [69]/with permission of John Wiley & Sons. (b) 2D isotropic shielding map of circumcoronene. Source: Reproduced from Zou et al. [70]/with permission of John Wiley & Sons.

literature, spanning from 2020 to the present, to appraise the (anti)aromatic nature of nanographenes.

Magnetic criteria are by far the most used to evaluate the aromaticity of nanographenes. More specifically, most of the recent literature reporting the analysis of new nanographene molecules employs a combination of ACID plots and single-point NICS calculations. As a representative example, Wu et al. analyzed in 2020 the electronic structure of two cove-edged graphene fragments, helping them to identify the anticipated Clar sextets (Figure 1.12a) [69]. In the case of planar systems like circumcoronene [70], synthesized very recently by the same group, the 2D variation of NICS is also suitable (Figure 1.12b). In this particular example, the authors complemented their analysis with HOMA calculations (geometric criteria) that supported the conclusions derived from magnetic methodologies. Notably, circumcoronene was further studied by Poranne et al. using the recently implemented NICS2BC method (see Figure 1.2), which employs NICS calculations represented as ring current graphs analogous to ACID plots [71].

When moving to the realm of contorted nanographenes, the 3D variations of NICS emerge as useful complements to single-point calculations. In this sense, Sundholm, Orozco-Ic et al. generated B_z^{ind} surfaces of [12]infinitene [72], a figure-eight contorted nanographene synthesized by Itami et al. in 2022 [73] (Figure 1.13a, top and bottom left). The analysis helped at identifying a shielding area (blue) along the whole

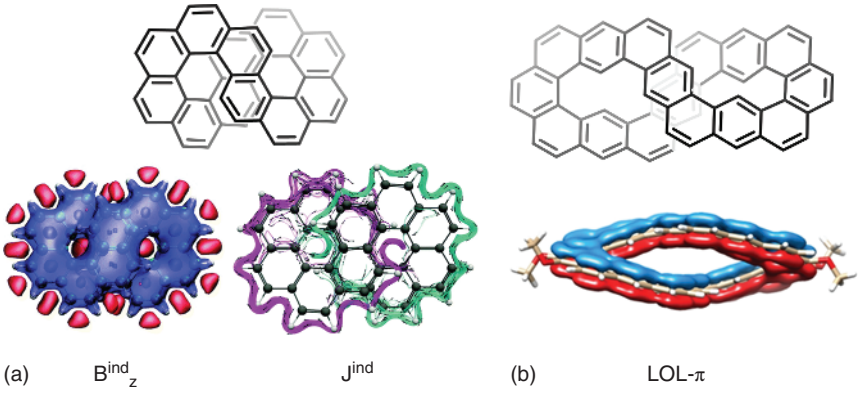

Figure 1.13 (a) Aromaticity analysis of [12]infinitene using B^{ind} surfaces (left) and GIMIC plots (right). Source: Orozco-Ic et al. [72]/Royal Society of Chemistry/CC BY 3.0. (b) LOL-π surface of a figure-eight fused [5]helicene dimer. Source: Reproduced from Zhou et al. [74]/with permission of John Wiley & Sons.

molecular structure together with local deshielding cones (red) in the middle of the loops, typical of helicene-containing systems. Most notably, the authors used the GIMIC method (Figure 1.13a, bottom right) to identify two independent current density pathways along the outer rim of the molecule that fulfill the rule of cylindrical aromaticity [72]. A related figure-eight molecule (Figure 1.13b, top) was reported by Wu et al. later on [74]. In this latter case, the aromaticity was analyzed according to the electronic criteria using the LOL-π, revealing delocalized π-orbitals along the whole structure (Figure 1.13b, bottom).

3D IMS maps were introduced recently [68] as an alternative to ICCS and B^{ind} isosurfaces for studying the aromaticity of highly contorted nanographene molecules relying on the magnetic criteria. Coquerel and co-workers [75] employed 3D IMS maps in combination with EDDB to analyze the aromaticity of an overcrowded triply fused carbo[7]helicene (Figure 1.14). The results showed a mismatch with the

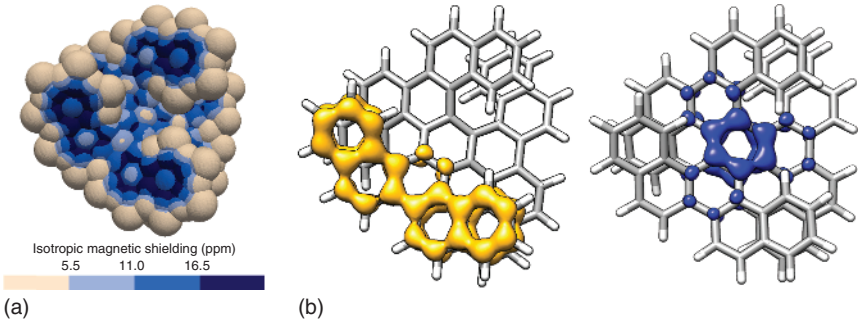

Figure 1.14 Aromaticity analysis of an overcrowded triply fused carbo[7]helicene using (a) a 3D IMS map and (b) $EDDB_F(r)$ isosurfaces. Source: Reproduced from Artigas et al. [75]/with permission of American Chemical Society.

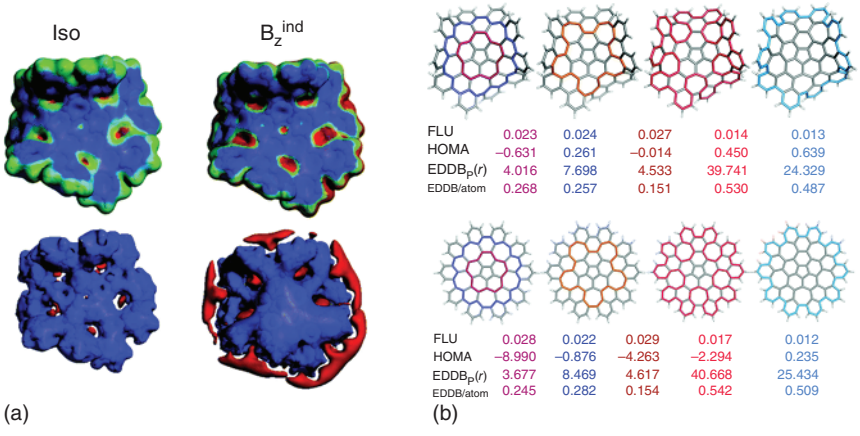

Figure 1.15 (a) Aromaticity analysis of Itami's grossly warped nanographene on the basis of magnetic criteria. (b) Analysis of the most favorable π-electron circuits on Itami's grossly warped nanographene on the basis of geometric criteria (HOMA) and electronic criteria. Source: Reproduced from Escayola et al. [78]/with permission of Royal Society of Chemistry.

anticipated Clar structure, probably emerging from the extremely contorted nature of the molecule.

The introduction of five- and seven-membered rings in the structure of nanographenes has been widely used over the last years to introduce curvature and to tune their electronic properties [76]. An exemplary case illustrating this approach is the so-called grossly warped nanographene, reported by Itami et al. in 2013 [77]. This π-extended corannulene features a central pentagon and five heptagons on its periphery whose global and local aromaticity was evaluated by Solà, Muñoz-Castro et al. in 2021 [78]. A comprehensive set of aromaticity indices was employed in the study, including 1D, 2D, and 3D variations of NICS, GIMIC, FLU, HOMA, MCI, and EDDB analyses. The authors unveiled a global 75 π-electron circuit on the edge of the molecule's backbone that does not follow any of the aromaticity rules (Figure 1.15).

1.5 Concluding Remarks

Nanographenes have distinct optoelectrical properties that make them indispensable for crafting state-of-the-art materials in technology. The quest for stability in nanographene design is paramount, and it relies on a complex interplay of factors, including size, structure, and functionalization. Aromaticity stands out as a critical contributor to the stabilization of nanographenes. Throughout our discussion, we have examined a plethora of techniques for measuring aromaticity in nanographenes and provide contemporary examples of their practical applications. In our opinion, the most fundamental descriptors of aromaticity are those that measure the energetic stabilization gained by aromaticity and the electron delocalization. For each indicator of aromaticity presented, we have collected

strengths and weaknesses. While magnetic criteria have been widely utilized in the literature, our analysis underscores that no single aromaticity descriptor is devoid of limitations, especially when considering magnetic indices. For this reason, it is advisable to employ at least two distinct aromaticity indicators rooted in different properties, with a preference for methods based on energetic or electron delocalization measures.

Acknowledgments

We thank the Spanish Ministerio de Ciencia e Innovación for projects PID2020-113711GB-I00, PID2023-147424NB-I00, and Margarita Salas grant (NextGenerationEU) to Albert Artigas and the Generalitat de Catalunya for project 2021SGR623.

References

1 Novoselov, K.S., Geim, A.K., Morozov, S.V. et al. (2004). Electric field effect in atomically thin carbon films. *Science* 306: 666–669.

2 Gu, Y., Qiu, Z., and Müllen, K. (2022). Nanographenes and graphene nanoribbons as multitalents of present and future materials science. *J. Am. Chem. Soc.* 144: 11499–11524.

3 (a) Wade, J., Salerno, F., Kilbride, R.C. et al. (2022). Controlling anisotropic properties by manipulating the orientation of chiral small molecules. *Nat. Chem.* 14: 1383–1389. (b) Huisman, K.H. and Thijssen, J.M. (2021). CISS effect: a magnetoresistance through inelastic scattering. *J. Phys. Chem. C* 125: 23364–23369. (c) Houska, V., Ukraintsev, E., Vacek, J. et al. (2023). Helicene-based π-conjugated macrocycles: their synthesis, properties, chirality and self-assembly into molecular stripes on a graphite surface. *Nanoscale* 15: 1542–1553. (d) Matxain, J.M., Ugalde, J.M., Mujica, V. et al. (2019). Chirality induced spin selectivity of photoexcited electrons in carbon-sulfur [*n*]helicenes. *ChemPhotoChem* 3: 770–777.

4 (a) Fujii, S. and Enoki, T. (2013). Nanographene and graphene edges: electronic structure and nanofabrication. *Acc. Chem. Res.* 46: 2202–2210. (b) Liu, J. and Feng, X. (2020). Synthetic tailoring of graphene nanostructures with zigzag-edged topologies: progress and perspectives. *Angew. Chem. Int. Ed.* 59: 23386–23401. (c) Song, S., Su, J., Telychko, M. et al. (2021). On-surface synthesis of graphene nanostructures with π-magnetism. *Chem. Soc. Rev.* 50: 3238–3262. (d) Pizzochero, M., Barin, G.B., Čerņevičs, K.N. et al. (2021). Edge disorder in bottom-up zigzag graphene nanoribbons: implications for magnetism and quantum electronic transport. *J. Phys. Chem. Lett.* 12: 4692–4696.

5 (a) Gröning, O., Wang, S., Yao, X. et al. (2018). Engineering of robust topological quantum phases in graphene nanoribbons. *Nature* 560: 209–213. (b) Rizzo,

D.J., Veber, G., Cao, T. et al. (2018). Topological band engineering of graphene nanoribbons. *Nature* 560: 204–208.

6 Soavi, G., Dal Conte, S., Manzoni, C. et al. (2016). Exciton–exciton annihilation and biexciton stimulated emission in graphene nanoribbons. *Nat. Commun.* 7: 11010.

7 (a) Fernández-García, J.M., Evans, P.J., Filippone, S. et al. (2019). Chiral molecular carbon nanostructures. *Acc. Chem. Res.* 52: 1565–1574. (b) Evans, P.J., Ouyang, J., Favereau, L. et al. (2018). Synthesis of a helical bilayer nanographene. *Angew. Chem. Int. Ed.* 57: 6774–6779. (c) Cruz, C.M., Castro-Fernández, S., Maçôas, E. et al. (2018). Undecabenzo[7]superhelicene: a helical nanographene ribbon as a circularly polarized luminescence emitter. *Angew. Chem. Int. Ed.* 57: 14782–14786. (d) Míguez-Lago, S., Mariz, I.F.A., Medel, M.A. et al. (2022). Highly contorted superhelicene hits near-infrared circularly polarized luminescence. *Chem. Sci.* 13: 10267–10272.

8 Merino, G., Solà, M., Fernández, I. et al. (2023). Aromaticity: quo Vadis. *Chem. Sci.* 14: 5569–5576.

9 Chen, Z., Wannere, C.S., Corminboeuf, C. et al. (2005). Nucleus-independent chemical shifts (NICS) as an aromaticity criterion. *Chem. Rev.* 105: 3842–3888.

10 Anderson, H.V., Gois, N.D., and Chalifoux, W.A. (2023). New advances in chiral nanographene chemistry. *Org. Chem. Front.* 10: 4167–4197.

11 Gershoni-Poranne, R. and Tsybizova, A. (2023). A crowning achievement: the first solution-phase synthesis of circumcoronenes. *Angew. Chem. Int. Ed.* 62: e202305289.

12 (a) Clar, E. (1972). *The Aromatic Sextet*. New York: Wiley; (b) Solà, M. (2013). *Front. Chem.* 1: 22.

13 Portella, G., Poater, J., Bofill, J.M. et al. (2005). Local aromaticity of [n]acenes, [n]phenacenes, and [n]helicenes (n = 1–9). *J. Org. Chem.* 70: 2509–2521.

14 Balaban, A.T. and Klein, D.J. (2009). Claromatic carbon nanostructures. *J. Phys. Chem. C* 113: 19123–19133.

15 Glidewell, C. and Lloyd, D. (1984). MNDO study of bond orders in some conjugated bi- and tri-cyclic hydrocarbons. *Tetrahedron* 40: 4455–4472.

16 Jirásek, M., Rickhaus, M., Tejerina, L., and Anderson, H.L. (2021). Experimental and theoretical evidence for aromatic stabilization energy in large macrocycles. *J. Am. Chem. Soc.* 143: 2403–2412.

17 Gilles, J.M., Oth, J.F.M., Sondheimer, F., and Woo, E.P. (1971). Unsaturated macrocyclic compounds. Part LXXXIII. A quantitative study of the conformational mobility of [18]annulene. *J. Chem. Soc. B Phys. Org.* 2177–2186.

18 Cyrański, M.K. (2005). Energetic aspects of cyclic π-electron delocalization: evaluation of the methods of estimating aromatic stabilization energies. *Chem. Rev.* 105: 3773–3811.

19 Casademont-Reig, I., Ramos-Cordoba, E., Torrent-Sucarrat, M., and Matito, E. (2020). How do the Hückel and Baird rules fade away in annulenes? *Molecules* 25: 711.

20 Soncini, A., Fowler, P.W., and Jenneskens, L.W. (2004). Ring currents in large [$4n+2$]-annulenes. *Phys. Chem. Chem. Phys.* 6: 277–284.

21 Kaiser, K., Scriven, L.M., Schulz, F. et al. (2019). An sp-hybridized molecular carbon allotrope, cyclo[18]carbon. *Science* 365: 1299–1301.

22 Stasyuk, A.J., Stasyuk, O.A., Solà, M., and Voityuk, A.A. (2020). Cyclo[18]carbon: the smallest all-carbon electron acceptor. *Chem. Commun.* 56: 352–355.

23 Poater, J., García-Cruz, I., Illas, F., and Solà, M. (2004). Discrepancy between common local aromaticity measures in a series of carbazole derivatives. *Phys. Chem. Chem. Phys.* 6: 314–318.

24 (a) Hehre, W.J., Ditchfiel, R., Radom, L., and Pople, J.A. (1970). Molecular orbital theory of electronic structure of organic compounds. 5. Molecular theory of bond separation. *J. Am. Chem. Soc.* 92: 4796–4801. (b) Pople, J.A., Radom, L., and Hehre, W.J. (1971). Molecular orbital theory of the electronic structure of organic compounds. VII. Systematic study of energies, conformations, and bond interactions. *J. Am. Chem. Soc.* 93: 289–300.

25 (a) George, P., Trachtman, M., Bock, C.W., and Brett, A.M. (1976). Homodesmotic reactions for the assessment of stabilization energies in benzenoid and other conjugated cyclic hydrocarbons. *J. Chem. Soc. Perkin Trans.* 2: 1222–1227. (b) George, P., Trachtman, M., Brett, A.M., and Bock, C.W. (1977). Comparison of various isodesmic and homodesmotic reaction heats with values derived from published ab initio molecular orbital calculations. *J. Chem. Soc. Perkin Trans.* 2: 1036–1047. (c) Wheeler, S.E., Houk, K.N., Schleyer, P.v.R., and Allen, W.D. (2009). A hierarchy of homodesmotic reactions for thermochemistry. *J. Am. Chem. Soc.* 131: 2547–2560.

26 (a) Cyrański, M.K., Krygowski, T.M., Katritzky, A.R., and Schleyer, P.v.R. (2002). To what extent can aromaticity be defined uniquely? *J. Org. Chem.* 67: 1333–1338. (b) Cyrański, M.K., Schleyer, P.v.R., Krygowski, T.M. et al. (2003). Facts and artifacts about aromatic stability estimation. *Tetrahedron* 59: 1657–1665.

27 Schleyer, P.v.R. and Pühlhofer, F. (2002). Recommendations for the evaluation of aromatic stabilization energies. *Org. Lett.* 4: 2873–2876.

28 Dobrowolski, M.A., Ciesielski, A., and Cyrański, M.K. (2011). On the aromatic stabilization of corannulene and coronene. *Phys. Chem. Chem. Phys.* 13: 20557–20563.

29 Cyranski, M.K., Howard, S.T., and Chodkiewicz, M.L. (2004). Bond energy, aromatic stabilization energy and strain in IPR fullerenes. *Chem. Commun.* 2458–2459.

30 Dobrowolski, M.A., Cyrański, M.K., and Wróbel, Z. (2016). Cyclic π-electron delocalization in non-planar linear acenes. *Phys. Chem. Chem. Phys.* 18: 11813–11820.

31 Dobrowolski, M.A., Cyrański, M.K., Merner, B.L. et al. (2008). Interplay of π-electron delocalization and strain in [*n*](2,7)pyrenophanes. *J. Org. Chem.* 73: 8001–8009.

32 (a) Matito, E. and Solà, M. (2009). The role of electronic delocalization in transition metal complexes from the electron localization function and the quantum theory of atoms in molecules viewpoints. *Coord. Chem. Rev.* 253: 647–665. (b) Feixas, F., Matito, E., Poater, J., and Solà, M. (2015). Quantifying aromaticity

with electron delocalisation measures. *Chem. Soc. Rev.* 44: 6434–6451. (c) Solà, M., Boldyrev, A.I., Cyrański, M.C. et al. (2023). *Aromaticity and Antiaromaticity: Concepts and Applications*. New York: Wiley-VCH.

33 (a) Fradera, X., Austen, M.A., and Bader, R.F.W. (1999). The Lewis model and beyond. *J. Phys. Chem. A* 103: 304–314. (b) Fradera, X., Poater, J., Simon, S. et al. (2002). Electron-pairing analysis from localization and delocalization indices in the framework of the atoms-in-molecules theory. *Theor. Chem. Accounts* 108: 214–224.

34 Mayer, I. (1986). Bond orders and valences from ab initio wave functions. *Int. J. Quantum Chem.* 29: 477–483.

35 (a) Matito, E., Duran, M., and Solà, M. (2005). The aromatic fluctuation index (FLU): a new aromaticity index based on electron delocalization. *J. Chem. Phys.* 122: 014109. (b) Matito, E., Duran, M., and Solà, M. (2006). Erratum: "The aromatic fluctuation index (FLU): a new aromaticity index based on electron delocalization" [J. Chem Phys. 122, 014109 (2005)]. *J. Chem. Phys.* 125: 059901.

36 Giambiagi, M., de Giambiagi, M.S., dos Santos, C.D., and de Figueiredo, A.P. (2000). Multicenter bond indices as a measure of aromaticity. *Phys. Chem. Chem. Phys.* 2: 3381–3392.

37 Bultinck, P., Ponec, R., and Van Damme, S. (2005). Multicenter bond indices as a new measure of aromaticity in polycyclic aromatic hydrocarbons. *J. Phys. Org. Chem.* 18: 706–718.

38 Cioslowski, J., Matito, E., and Solà, M. (2007). Properties of aromaticity indices based on the one-electron density matrix. *J. Phys. Chem. A* 111: 6521–6525.

39 (a) Feixas, F., Matito, E., Poater, J., and Solà, M. (2008). On the performance of some aromaticity indices: a critical assessment using a test set. *J. Comput. Chem.* 29: 1543–1554. (b) Feixas, F., Jiménez-Halla, J.O.C., Matito, E. et al. (2010). A test to evaluate the performance of aromaticity descriptors in all-metal and semimetal clusters. An appraisal of electronic and magnetic indicators of aromaticity. *J. Chem. Theory Comput.* 6: 1118–1130.

40 (a) Bader, R.F.W. (1985). Atoms in molecules. *Acc. Chem. Res.* 18: 9–15. (b) Bader, R.F.W. (1990). *Atoms in Molecules: A Quantum Theory*. Oxford: Clarendon. (c) Bader, R.F.W. (1991). A quantum theory of molecular structure and its applications. *Chem. Rev.* 91: 893–928. (d) Matta, C.F. and Boyd, R.J. (ed.) (2007). *The Quantum Theory of Atoms in Molecules. From Solid State to DNA and Drug Design*. Weinheim: Wiley-VCH Verlag GmbH & Co. KGaA.

41 Poater, J., Duran, M., Solà, M., and Silvi, B. (2005). Theoretical evaluation of electron delocalization in aromatic molecules by means of atoms in molecules (AIM) and electron localization function (ELF) topological approaches. *Chem. Rev.* 105: 3911–3947.

42 Becke, A.D. and Edgecombe, K.E. (1990). A simple measure of electron localization in atomic and molecular systems. *J. Chem. Phys.* 92: 5397–5403.

43 (a) Santos, J.C., Andres, J., Aizman, A., and Fuentealba, P. (2005). An aromaticity scale based on the topological analysis of the electron localization function including σ and π contributions. *J. Chem. Theor. Comput.* 1: 83–86. (b) Santos,

J.C., Tiznado, W., Contreras, R., and Fuentealba, P. (2004). *Sigma-pi* separation of the electron localization function and aromaticity. *J. Chem. Phys.* 120: 1670–1673.

44 (a) Schmider, H.L. and Becke, A.D. (2000). Chemical content of the kinetic energy density. *J. Mol. Struct. (THEOCHEM)* 527: 51–61. (b) Tsirelson, V. and Stash, A. (2002). Analyzing experimental electron density with the localized-orbital locator. *Acta Crystallogr. B* 58: 780–785. (c) Jacobsen, H. (2008). Localized-orbital locator (LOL) profiles of chemical bonding. *Can. J. Chem.* 86: 695–702.

45 Liu, Z., Lu, T., Hua, S., and Yu, Y. (2019). Aromaticity of Hückel and Möbius topologies involved in conformation conversion of macrocyclic [32]Octaphyrin(1.0.1.0.1.0.1.0): refined evidence from multiple visual criteria. *J. Phys. Chem. C* 123: 18593–18599.

46 Szczepanik, D.W. (2016). A new perspective on quantifying electron localization and delocalization in molecular systems. *Comput. Theor. Chem.* 1080: 33–37.

47 Szczepanik, D.W., Solà, M., Krygowski, T.M. et al. (2018). Aromaticity of acenes: the model of migrating π-circuits. *Phys. Chem. Chem. Phys.* 20: 13430–13436.

48 Szczepanik, D.W. and Solà, M. (2021). *Aromaticity: Modern Computational Methods and Applications* (ed. I. Fernandez), 259–284. Dordrecht: Elsevier.

49 (a) Kruszewski, J. and Krygowski, T.M. (1972). Definition of aromaticity basing on the harmonic oscillator model. *Tetrahedron Lett.* 13: 3839–3842. (b) Krygowski, T.M. (1993). Crystallographic studies of inter- and intra-molecular interactions reflected in benzenoid hydrocarbons. nonequivalence of indices of aromaticity. *J. Chem. Inf. Comp. Sci.* 33: 70–78. (c) Krygowski, T.M. and Cyrański, M.K. (2001). Structural aspects of aromaticity. *Chem. Rev.* 101: 1385–1419.

50 Zborowski, K.K., Alkorta, I., Elguero, J., and Proniewicz, L.M. (2012). Calculation of the HOMA model parameters for the carbon–boron bond. *Struct. Chem.* 23: 595–600.

51 Zborowski, K.K., Alkorta, I., Elguero, J., and Proniewicz, L.M. (2013). HOMA parameters for the boron–boron bond: how the introduction of a BB bond influences the aromaticity of selected hydrocarbons. *Struct. Chem.* 24: 543–548.

52 Krygowski, T.M. and Cyrański, M.K. (1996). Separation of the energetic and geometric contributions to the aromaticity of π-electron carbocyclics. *Tetrahedron* 52: 1713–1722.

53 Sundholm, D., Fliegl, H., and Berger, R.J.F. (2016). Calculations of magnetically induced current densities: theory and applications. *WIREs Comput. Mol. Sci.* 6: 639–678.

54 Fliegl, H., Taubert, S., Lehtonen, O., and Sundholm, D. (2011). The gauge including magnetically induced current method. *Phys. Chem. Chem. Phys.* 13: 20500–20518.

55 Herges, R. and Geuenich, D. (2001). Delocalization of electrons in molecules. *J. Phys. Chem. A* 105: 3214–3220.

56 Geuenich, D., Hess, K., Köhler, F., and Herges, R. (2005). Anisotropy of the induced current density (ACID), a general method to quantify and visualize electronic delocalization. *Chem. Rev.* 105: 3758–3772.

57 Han, Y., Xue, Z., Li, G. et al. (2020). Formation of azulene-embedded nanographene: naphthalene to azulene rearrangement during the Scholl reaction. *Angew. Chem. Int. Ed.* 59: 9026–9031.

58 (a) Bühl, M. and van Wüllen, C. (1995). Computational evidence for a new C_{84} isomer. *Chem. Phys. Lett.* 247: 63–68. (b) Schleyer, P.v.R., Maerker, C., Dransfeld, A. et al. (1996). Nucleus-independent chemical shifts: a simple and efficient aromaticity probe. *J. Am. Chem. Soc.* 118: 6317–6318.

59 (a) Corminboeuf, C., Heine, T., Seifert, G. et al. (2004). Induced magnetic fields in aromatic [*n*]-annulenes – interpretation of NICS tensor components. *Phys. Chem. Chem. Phys.* 6: 273–276. (b) Schleyer, P.v.R., Manoharan, M., Jiao, H.J., and Stahl, F. (2001). The acenes: is there a relationship between aromatic stabilization and reactivity? *Org. Lett.* 3: 3643–3646.

60 Fallah-Bagher-Shaidaei, H., Wannere, C.S., Corminboeuf, C. et al. (2006). Which NICS aromaticity index for planar rings is best? *Org. Lett.* 8: 863–866.

61 (a) Lazzeretti, P. (2000). Ring currents. *Prog. Nucl. Magn. Res. Spectrum* 36: 1–88. (b) Lazzeretti, P. (2004). Assessment of aromaticity via molecular response properties. *Phys. Chem. Chem. Phys.* 6: 217–223. (c) Aihara, J. (2002). Nucleus-independent chemical shifts and local aromaticities in large polycyclic aromatic hydrocarbons. *Chem. Phys. Lett.* 365: 34–39. (d) Poater, J., Solà, M., Viglione, R.G., and Zanasi, R. (2004). Local aromaticity of the six-membered rings in pyracylene. A difficult case for the NICS indicator of aromaticity. *J. Org. Chem.* 69: 7537–7542. (e) Islas, R., Martínez-Guajardo, G., Jiménez-Halla, J.O.C. et al. (2010). Not all that has a negative NICS is aromatic: the case of the H-bonded cyclic trimer of HF. *J. Chem. Theory Comput.* 6: 1131–1135. (f) Havenith, R.W.A., De Proft, F., Fowler, P.W., and Geerlings, P. (2005). σ-Aromaticity in H_3^+ and Li_3^+: insights from ring-current maps. *Chem. Phys. Lett.* 407: 391–396. (g) Van Damme, S., Acke, G., Havenith, R.W.A., and Bultinck, P. (2016). Can the current density map topology be extracted from the nucleus independent chemical shifts? *Phys. Chem. Chem. Phys.* 18: 11746–11755. (h) Fias, S., Van Damme, S., and Bultinck, P. (2008). Multidimensionality of delocalization indices and nucleus independent chemical shifts in polycyclic aromatic hydrocarbons. *J. Comput. Chem.* 29: 358–366. (i) Zhao, L., Grande-Aztatzi, R., Foroutan-Nejad, C. et al. (2017). Aromaticity, the Hückel 4*n*+2 rule and magnetic current. *ChemistrySelect* 2: 863–870.

62 Gershoni-Poranne, R. and Stanger, A. (2014). The NICS-XY-scan: identification of local and global ring currents in multi-ring systems. *Chem. Eur. J.* 20: 5673–5688.

63 Muñoz-Castro, A. (2017). The shielding cone in spherical aromatic structures: insights from models for spherical $2(N+1)^2$ aromatic fullerenes. *Phys. Chem. Chem. Phys.* 19: 12633–12636.

64 Karadakov, P.B., Hearnshaw, P., and Horner, K.E. (2016). Magnetic shielding, aromaticity, antiaromaticity, and bonding in the low-lying electronic states of benzene and cyclobutadiene. *J. Org. Chem.* 81: 11346–11352.

65 Lampkin, B.J., Karadakov, P.B., and VanVeller, B. (2020). Detailed visualization of aromaticity using isotropic magnetic shielding. *Angew. Chem. Int. Ed.* 59: 19275–19281.

66 Klod, S. and Kleinpeter, E. (2001). Ab initio calculation of the anisotropy effect of multiple bonds and the ring current effect of arenes—application in conformational and configurational analysis. *J. Chem. Soc. Perkin Trans.* 2: 1893–1898.

67 (a) Merino, G., Vela, A., and Heine, T. (2005). Description of electron delocalization via the analysis of molecular fields. *Chem. Rev.* 105: 3812–3841. (b) Islas, R., Heine, T., and Merino, G. (2012). The induced magnetic field. *Acc. Chem. Res.* 45: 215–228.

68 Artigas, A., Hagebaum-Reignier, D., Carissan, Y., and Coquerel, Y. (2021). Visualizing electron delocalization in contorted polycyclic aromatic hydrocarbons. *Chem. Sci.* 12: 13092–13100.

69 Gu, Y., Muñoz-Mármol, R., Wu, S. et al. (2020). Cove-edged nanographenes with localized double bonds. *Angew. Chem. Int. Ed.* 59: 8113–8117.

70 Zou, Y., Hou, X., Wei, H. et al. (2023). Circumcoronenes. *Angew. Chem. Int. Ed.* 62: e202301041.

71 Paenurk, E. and Gershoni-Poranne, R. (2022). Simple and efficient visualization of aromaticity: bond currents calculated from NICS values. *Phys. Chem. Chem. Phys.* 24: 8631–8644.

72 Orozco-Ic, M., Valiev, R.R., and Sundholm, D. (2022). Non-intersecting ring currents in [12]infinitene. *Phys. Chem. Chem. Phys.* 24: 6404–6409.

73 Krzeszewski, M., Ito, H., and Itami, K. (2022). Infinitene: a helically twisted figure-eight [12]Circulene topoisomer. *J. Am. Chem. Soc.* 144: 862–871.

74 Zhou, Q., Hou, X., Wang, J. et al. (2023). A fused [5]Helicene dimer with a figure-eight topology: synthesis, chiral resolution, and electronic properties. *Angew. Chem. Int. Ed.* 62: e202302266.

75 Artigas, A., Rigoulet, F., Giorgi, M. et al. (2023). Overcrowded triply fused carbo[7]helicene. *J. Am. Chem. Soc.* 145: 15084–15087.

76 Majewski, M.A. and Stępień, M. (2019). Bowls, hoops, and saddles: synthetic approaches to curved aromatic molecules. *Angew. Chem. Int. Ed.* 58: 86–116.

77 Kawasumi, K., Zhang, Q., Segawa, Y. et al. (2013). A grossly warped nanographene and the consequences of multiple odd-membered-ring defects. *Nat. Chem.* 5: 739–744.

78 Escayola, S., Poater, A., Muñoz-Castro, A., and Solà, M. (2021). An unprecedented π-electronic circuit involving an odd number of carbon atoms in a grossly warped non-planar nanographene. *Chem. Commun.* 57: 3087–3090.